LAWRENCE
LIVERMORE
NATIONAL
LABORATORY

LLNL-JRNL-669215

Mesoscale Evolution of Voids and Microstructural Chagnes in HMX-based Explosives During Heating Through the beta-delta Phase Transition

T. M. Willey, L. Lauderbach, F. Gagliardi, T. van Buuren, E. A. Glascoe, J. W. Tringe, J. R. I. Lee, K. Springer, J. Ilavsky

March 31, 2015

Journal of Applied Physics

Disclaimer

Mesoscale Evolution of Voids and Microstructural Changes in HMX-based Explosives during Heating Through the β-δ Phase Transition

Trevor M. Willey, Lisa Lauderbach, Franco Gagliardi, Tony van Buuren,
Elizabeth A. Glascoe, Joseph W. Tringe, Jonathan R. I. Lee, and Keo Springer
Lawrence Livermore National Laboratory, Livermore CA 94550

Jan Ilavsky
Argonne National Laboratory, Argonne IL

HMX-based explosives LX-10 and PBX-9501 were heated through the β-δ phase transition. Ultra-small angle x-ray scattering (USAXS), recorded as the HMX was heated, indicate how the void volume and mesoscale structure of the explosive changes due to the phase transition. Molecular diffraction was simultaneously recorded to ascertain the phase of the HMX during the heating cycle. X-ray induced damage, observed in the USAXS, occurs more readily at elevated temperatures; as such, the dose was reduced to mitigate this effect. Optical microscopy performed during a similar heating cycle gives an indication of changes on longer length scales, while x-ray microtomography, performed before and after heating, shows the character of extensive microstructural damage resulting from the temperature cycle and solid-state phase transition.

Introduction

Octahydro-1,3,5,7-tetranitro-1,3,5,7-tetrazocine, also known as HMX or octogen, exhibits a solid-solid phase β-δ transition at around 160-180 °C. HMX-based explosives heated through the β-δ phase transition exhibit increased shock sensitivity[1]. HMX-based explosives also "cook-off" at elevated temperatures above this phase transition, when self-heating from exothermic reactions leads to deflagration and even detonation[2-5]. The sensitivity is qualitatively attributed to two factors: the lower thermal stability of the δ-phase[6], as well as increased hot spots[7, 8] and initiation centers from voids and porosity created during the phase transition. Quantification of how mesoscale (~10nm to ~1 μm) voids affect sensitivity requires experimental measurement of such porosity during heating to address open questions regarding physiochemical processes that govern HMX sensitivity[6] and to provide experimental validation and/or input to modeling[9-11].

This work used a combination of ultra-small angle x-ray scattering (USAXS) optical microscopy, and x-ray microtomography to investigate mesoscale and microstructural changes during heating and particularly due to the β-δ phase transition. The USAXS and microscopy were performed as the explosive was heated through the phase transition. Tomography was performed on the same explosives before and after heating.

Experimental

To quantify mesoscale changes influencing sensitivity, we performed USAXS/SAXS on HMX-based LX-10 (95% HMX, 5% Viton), PBX-9501 (95wt. % HMX, with 2.5wt. % Estane, 1.25 wt. % BDNPA (bis(2,2-dinitropropyl)acetal), and 1.25 wt. % BDNPF (bis(2,2-dinitropropyl) formal)), and single crystals of HMX. The PBX materials were pressed between 0.7 and 0.8 mm thick, and subsequently laser-cut to about 2.0 mm in diameter, leading to sample masses of about 10 mg. A Linkam THMS600 modified for x-ray scattering was used to heat and control the temperature of the explosive. Pellets were placed between two thin layers of Kapton, and held radially unconfined against the heater and x-ray aperture with a spring clip.

The USAXS experiments were performed at 15-ID-D at the Advanced Photon Source at Argonne National Laboratory using the upgraded USAXS instrument[12]. This instrument now has the capability to acquire scattering from 10^{-4} Å^{-1} to 2 Å^{-1} by automatically sequentially acquiring Bonse-Hart USAXS and conventional SAXS/WAXS. Data were processed using the Irena, Indra, and Nika SAXS reduction and analysis codes[13, 14].

These measurements, during heating, contrast previous studies that acquired SAXS before heating and/or after returning HMX-based samples to ambient temperatures[15-17]. Microscopy on these explosives was also performed in the Linkam heating stage. X-ray computed tomography performed at beamline 8.3.2 at the Advanced Light Source[18] was used to investigate the internal damage in the explosives.

Inhomogeneities in electron density give rise to small angle scattering. Small angle X-ray scattering (SAXS) is sensitive to structural inhomogeneities with dimensions between ~ 1 nm and 5 μm and, as such, is ideally suited to studying the size and size dispersion of voids in high explosives. A comprehensive treatment of the theoretical basis for obtaining this information from a scattering profile lies beyond the scope of this paper and can be found elsewhere in the literature[19]; nonetheless, we present a brief overview of the key processes and equations that define the scattering profile.

In its simplest form, the scattered intensity is the square of the Fourier transform of the scattering length density: $\rho(\mathbf{r})$

$$I(q) = \left| \int \rho(\mathbf{r}) e^{-iq\mathbf{r}} \, d\mathbf{r} \right|^2 \quad (1)$$

where $q = \frac{4\pi}{\lambda}\sin(\theta)$, with λ as the wavelength of scattered radiation, and θ is the scattering half angle. The scattering density in a unit cell can be represented by a scattering density function, $\rho_u(\mathbf{r})$; the spatial distribution of the scattering sights is given by $z(\mathbf{r})$. The total scattering length density is a convolution of these two terms: $\rho(\mathbf{r}) = \rho_u(\mathbf{r}) * z(\mathbf{r})$. This leads to the scattering intensity: $I(q) \propto f(q)S(q)$, where $f(q)$, the general scattering form factor arises from $\rho_u(\mathbf{r})$, and the structure factor $S(q)$ comes from $z(\mathbf{r})$. Assuming dilute voids with uncorrelated positions and random orientation, $S(q)$ is constant equal to unity, and the scattering is only a function of the form factor. In this approximation, scattering can be written in the following form:

$$I(q) = |\Delta\rho|^2 \int_0^\infty \left| F(q,s) \right|^2 V^2(s) NP(s) ds \quad (2)$$

In Eq. 2, s is the size of the scattering particle, $\Delta\rho$ is the scattering contrast (related to the difference in electron density) between the scatterer and its surroundings, $F(q,s)$ is the scattering form factor, $V(s)$ is the volume of the particle, N is the total number of particles, and $P(s)$ is the probability of having a scatterer of size s (the scattering size distribution function).

Although $\rho(\mathbf{r})$ gives a unique scattering intensity profile, the inverse is not unique. Therefore, eq. 2 must be used to generate the scattering based on an assumed form factor and size distribution of particles. For this study, the voids were modeled using a form factor for spheres. Furthermore, we assumed that the voids were randomly and uniformly dispersed throughout the explosive.

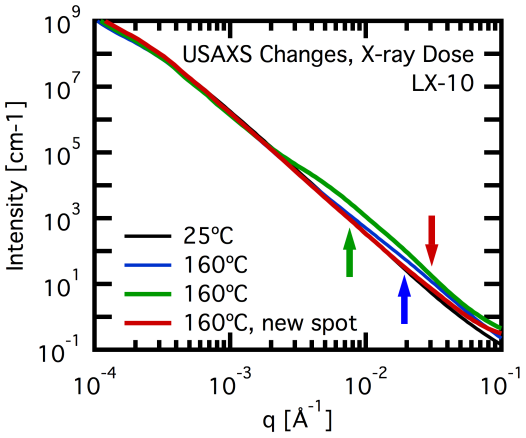

Figure 1: USAXS from LX-10. X-ray flux was first attenuated such that no appreciable changes were noted during the acquisition over ten USAXS traces. In this figure, three USAXS traces acquired at the same sample position at 25, 160, and 160°C show changes and evolution in the SAXS (blue & green arrows), while moving to a new sample position returns the USAXS trace to the same shape as the undamaged 25°C scan (red arrow), except for at the very highest q range, ~10^{-1} Å^{-1}.

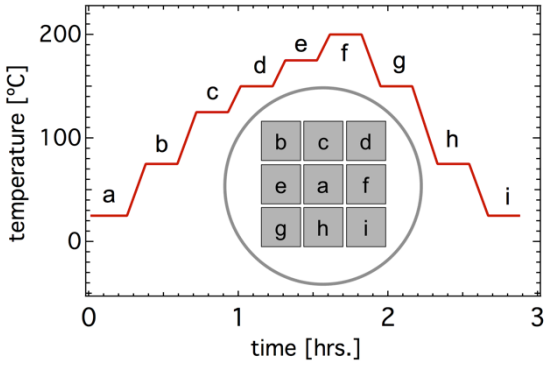

Figure 2: Temperature of the sample vs. time; USAXS profiles were acquired at each temperature a-i. Each acquisition illuminated a 0.4 x 0.4 mm area on the sample; a fresh point used for each acquisition as indicated in the diagram.

Results

During initial heating studies, the USAXS showed x-ray dose related changes to HMX crystallites, particularly at elevated temperature. The x-ray dose was reduced so that ten USAXS traces acquired in rapid succession from the same volume of the sample showed no appreciable changes in the USAXS. This dose was ultimately found to be an acceptable compromise between acquisition signal-to-noise, speed, and beam damage at elevated temperature. This flux was tested at 160°C; this test is outlined in figure 1. First, a USAXS trace was acquired at room temperature. The sample was then heated to 160°C, and two additional USAXS traces where acquired. The USAXS develops a Guinier in the first 160°C acquisition at ~2x10^{-2} Å^{-1}, which then moves to lower scattering angle, ~8x10^{-3} Å^{-1}, and intensifies in the subsequent trace. The x-ray beam was moved to an unexposed area of the sample, and the 160°C USAXS trace was again acquired. The trace matched the undamaged room temperature acquisition between 10^{-4} and 7x10^{-2} Å^{-1}, showing that for rapid acquisitions on unexposed areas, USAXS can be acquired with minimal beam-induced changes in this particular range. Above about 7x10^{-2} Å^{-1} and nearing the noise floor of the USAXS instrument, throughout our scans some additional intensity exists at elevated temperature and is presumably arises from the same temperature/x-ray exposure.

The temperature profile used in these studies and approximate beam positions within the Linkam aperture on the sample, labeled a-i on both, are depicted in Figure 2. Sample temperature was held constant during USAXS and SAXS acquisitions and ramped between scans at the rate indicated.

Concurrent to mesoscale porosity measurements, the regime at high scattering angle (0.9 – 1.4 Å^{-1}) monitors the phase of the HMX in LX-10 and PBX-9501 through molecular diffraction peaks. These are depicted in the top panes of Fig. 2 and correspondingly labeled a-i as in Fig. 1. Although peak intensities may vary as HMX crystallites have varying average orientations in each new sampling point, the diffraction shows the solid-solid β-δ phase transition[20, 21] occurs between acquisitions e

and f, as the temperature is ramped from 175 to 200°C. Further, the explosive remains in the δ-phase when cooled back to room temperature during this cycle.

Figure 3 present s the USAXS (middle panes) and USAXS-derived void volume distributions[13] (bottom panes.) The USAXS, sensitive to scattering from objects or voids ~10 nm to ~5 *u*m, shows relatively stable LX-10 and PBX-9501 mesoscale structure upon heating from 25° C to about 175° C. A dramatic scattering change occurs promptly with the β-δ phase transition. Scattering is greater throughout the entire q-range in all scans after the transition as depicted in 200° C and later δ- phase scans particularly at low (~10^{-4}) and high (10^{-1} $Å^{-1}$) q-ranges. This increased scattering implies a dramatic increase in void volume within the material. The scattering upon cooling in the LX-10 does not change appreciably while in PBX-9501 the scattering continues to increase during cooling. As noted previously, both samples remained in the δ-phase upon cooling at these timescales.

The power law slope at ~$5x10^{-3}$ $Å^{-1}$ is most shallow prior to heating at -3.7, while heated samples increase in slope. While this -3.7 slope does not unambiguously give morphology information, it does indicate that the low-q scattering centers either possess surface texture, are not fully three-dimensional (somewhat disk-like or rod-like characteristics) or have a broad size distribution extending towards smaller sizes. Similar features were observed in PBX-9501 and single-crystal HMX. Upon heating, the increase in slope to essentially -4 indicates a smoother interface, narrowing of the size distribution, and/or evolution towards more spherically shaped scatterers.

The lower panes of Fig. 3 present USAXS-derived void volume distributions[13] assuming spherical, randomly dispersed voids. Three positions a, f, and i (Fig. 1) at temperatures of 25° C, 200° C, and 25° C are presented for clarity. Prior to the phase transition both have broad size distributions with sizes of thousands of Ångstroms using this model. Post phase transition, this distribution breaks into a bimodal distribution with peaks ~10^3 and ~10^4 Å.

The LX-10 USAXS-derived void volume[13] started at 1.3%, hits 7% at 200° C, and increases to 8% after cooling back to 25° C. Voids in PBX-9501 started at 1.7%, increased to 9% post-transition, and then continued to increase to 12% upon cooling. The void increases are slightly larger but comparable to measured density changes in similar explosives undergoing the phase change[1].

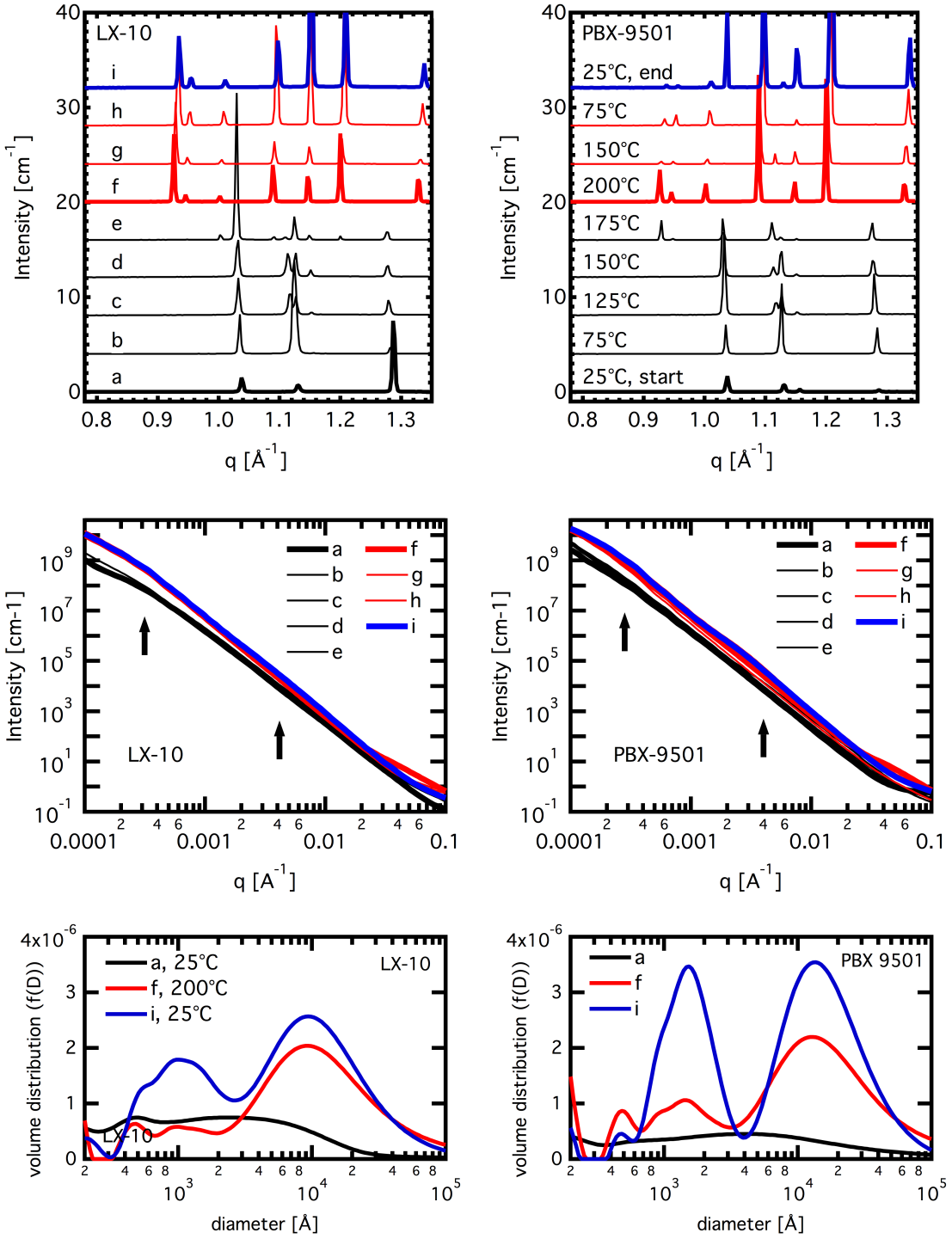

Figure 3: Top: Molecular diffraction from LX-10 and PBX-9501 samples during heating; positions and temperatures as listed in Fig. 1. Middle: USAXS data following the same color pattern. Bottom: Derived size distributions assuming a spherical model for voids.

Figure 4 shows optical microscopy images acquired during a similar temporal heating cycle. The left pane was acquired right before the β-δ phase transition (position e, Fig. 1); the middle pane was acquired right after the phase transition (between e and f); the right pane was acquired a few minutes after the phase transition, but prior to cooling (f). Prominent cracks appear at the interfaces that are several microns thick, and several hundred microns long as seen in the middle pane, Fig. 4. These cracks, however, rapidly disappear in the warm explosive. Although many of the features and crystallites of the β-phase (left pane) are still recognizable in the δ-phase of the right pane, crystallites have taken on different shapes and orientations, and some, especially smaller crystallites, are no longer visible post phase transition in the right frame.

Microtomography (Fig. 5) performed before and after USAXS experiments, shows extensive cracking forming in the sample due to the heating cycle. Note that tomography acquisitions were acquired several days before, and several days after the USAXS acquisition, and the post-temperature cycle sample, after several days, has likely reverted from the δ to the β phase. The observed cracking occurs primarily but not exclusively at crystallite boundaries at larger (>5 μm) length scales. The slices before and after heating could not be registered, even with fiducials placed on the samples. The lack of similarity in the tomography data before and after heating indicates extensive changes occur in mm-scale crystallite morphology during the temperature cycle.

Discussion

The β-δ phase transition alters the mesoscale voids and microstructure of HMX-based PBXs in dramatic fashion. The β-phase void distributions in LX-10 and PBX-9501 are broad over the 10 nm to 5 μm size regimes, and remain relatively stable upon heating, so long as the HMX remains in the β- phase. A prompt and dramatic change to the x-ray scattering occurs simultaneously with the change to δ-phase. In the raw USAXS, two curves appear with the phase change, and using a spherical model, the void volume with size breaks into a strongly bimodal distribution particularly in the PBX-9501, with peaks ~100 nm and ~1 μm. This data alone cannot conclusively establish spherical scatterers, but two distinct curves in the USAXS indicate new scattering on these length scales. Upon cooling, the void volume as seen in the distribution increases slightly in the LX-10, but dramatically in the PBX-9501. We postulate this is due to either weaker adhesion to HMX and/or decomposition of the Estane and plasticizer used in the PBX-9501.

At longer length scales and at later times, the temperature cycle leaves fissures along HMX crystallite boundaries as apparent in the LX-10 post-heating sample in the top-right of Figs. 5 and 6. However, in the optical microscopy of the heated HMX, apparently the viscous binders in LX-10 (Fig. 4) and/or dissolved and re-solidifying HMX[22] continue to and fill fissures created by the phase change at elevated temperature. We postulate much of the structure in the tomography forms in cooled PBXs that are initially in the δ phase with high-viscosity room temperature binders surrounding HMX crystals that revert to

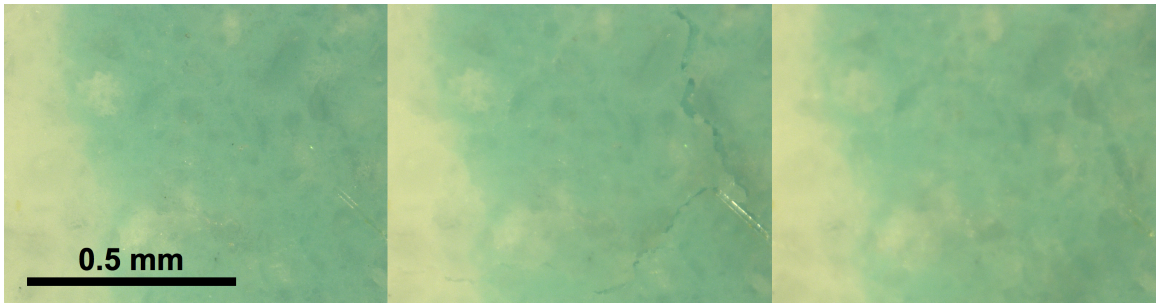

Figure 4: Optical microscopy images of LX-10, sequentially from left to right. Left pane: beta phase just before the beta-delta transition. Middle pane: Delta phase right after the transition, with visible fissures present. Many crystallites have changed shape and/or orientation. Right pane: Delta phase a few minutes after the transition; fissures have healed, presumably due to viscous binders in the PBX.

the β-phase over longer timescales[23], leaving fissures at crystallite boundaries. The PBX-9501 clearly has many more fissures encompassing a much larger portion of the volume; as with the mesoscale voids, we attribute the more prevalent fissures to either decomposition and/or weaker adhesion of the binder to HMX crystallites.

Summary and Conclusions

Small-angle scattering shows the most dramatic change in porosity occurs promptly with the β-δ phase transition with a large increase (in this case from ~1.3% to ~7% for LX-10) in mostly micron-scale porosity. The β-δ phase transition rather than heating itself is responsible for changes to mesoscale structure at elevated temperatures. At longer length and timescales, x-ray tomography and microscopy show fissures form at crystallite boundaries; at elevated temperatures, these are at least partially healed by flow in the binders, but are very dramatic in explosives that have been heated and then cooled to ambient for several days and likely reverted from the δ to the β phase. The prompt changes at the β-δ transition and then more protracted subsequent changes are key to quantifying how the β-δ phase change damages HMX crystallites. The experimental measurement of new porosity is key to isolating how voids vs. other phenomena affect the shock sensitivity of HMX at elevated temperatures.

Acknowledgements

The authors thank I. Tran, LLNL, for assistance during USAXS experiments, and D. Parkinson, ALS, LBNL, for assistance during tomography experiments, and C. Divin, LLNL, for acquiring x-ray nanotomography on single HMX crystals. This research was partially supported by the Joint DoD-DOE Munitions Technology Development Program. This work was performed under the auspices of the U.S. Department of Energy by Lawrence Livermore National Laboratory under Contract DE-AC52-07NA27344. ChemMatCARS Sector 15 is supported by the National Science Foundation/Department of Energy under grant number NSF/CHE-1346572. Use of the Advanced Photon Source, an Office of Science User Facility operated for the U.S. Department of Energy (DOE) Office of Science by Argonne National Laboratory, was supported by the U.S. DOE under Contract No. DE-AC02-06CH11357. The Advanced Light Source is supported by the Director, Office of Science,

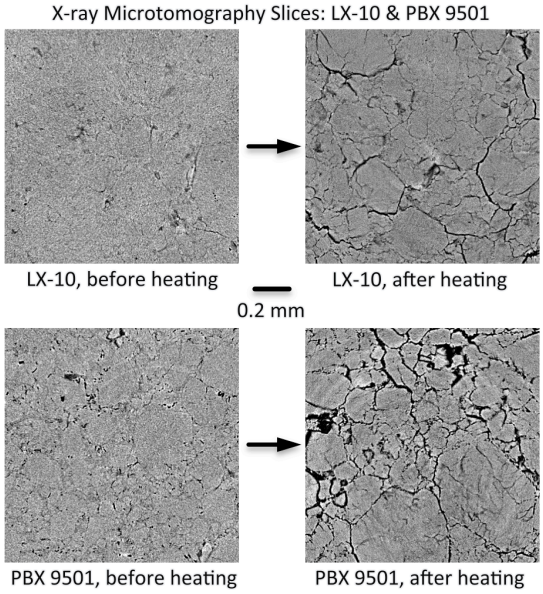

Figure 5: X-ray microtomography slice from LX-10 before and after heating. Cracking occurs throughout the sample.

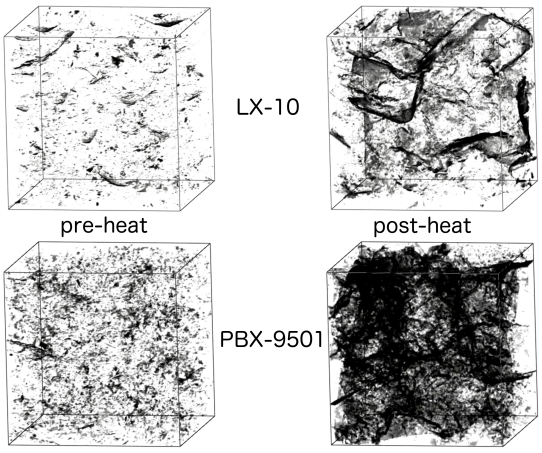

Figure 6: Three-dimensional renderings of cracks and voids in LX-10 and PBX-9501 before and after heating. Each of the cubes is 0.66 mm on a side.

Office of Basic Energy Sciences, of the U.S. Department of Energy under Contract No. DE-AC02-05CH11231. A condensed subset of the data presented herein and a preliminary analysis of this data appeared in the Proceedings of the International Detonation Symposium[24].

References:

1. Urtiew, P.A., et al., *Shock sensitivity of LX-04 containing delta phase HMX at elevated temperatures*, in *Shock Compression of Condensed Matter - 2003, Pts 1 and 2, Proceedings*, M.D. Furnish, Y.M. Gupta, and J.W. Forbes, Editors. 2004, Amer Inst Physics: Melville. p. 1053-1056.
2. Tarver, C.M. and T.D. Tran, *Thermal decomposition models for HMX-based plastic bonded explosives.* Combustion and Flame, 2004. **137**(1-2): p. 50-62.
3. Urtiew, P.A., et al., *Thermal cook-off of an HMX based explosive: Pressure gauge experiments and modeling.* Russian Journal of Physical Chemistry B, 2007. **1**(1): p. 46-51.
4. Yoh, J.J.I., et al., *Test-based thermal explosion model for HMX.* Proceedings of the Combustion Institute, 2007. **31**: p. 2353-2359.
5. Tarver, C.M. and J.G. Koerner, *Effects of endothermic binders on times to explosion of HMX- and TATB-Based plastic bonded explosives.* Journal of Energetic Materials, 2008. **26**(1): p. 1-28.
6. Sharia, O., R. Tsyshevsky, and M.M. Kuklja, *Surface-Accelerated Decomposition of delta-HMX.* Journal of Physical Chemistry Letters, 2013. **4**(5): p. 730-734.
7. Hatano, T., *Spatiotemporal behavior of void collapse in shocked solids.* Physical Review Letters, 2004. **92**(1): p. 015503.
8. Risse, B., F. Schnell, and D. Spitzer, *Synthesis and Desensitization of Nano-beta-HMX.* Propellants Explosives Pyrotechnics, 2014. **39**(3): p. 397-401.
9. Duan, X.H., et al., *Molecular dynamics simulations of void defects in the energetic material HMX.* Journal of Molecular Modeling, 2013. **19**(9): p. 3893-3899.
10. Springer, H.K., et al., *Investigating short-pulse shock initiation in HMX-based explosives with reactive meso-scale simulations.* 18th Aps-Sccm and 24th Airapt, Pts 1-19, 2014. **500**.
11. Menikoff, R. and T.D. Sewell, *Constituent properties of HMX needed for mesoscale simulations.* Combustion Theory and Modelling, 2002. **6**(1): p. 103-125.
12. Ilavsky, J., et al., *Ultra-small-angle X-ray scattering at the Advanced Photon Source.* Journal of Applied Crystallography, 2009. **42**: p. 469-479.
13. Ilavsky, J. and P.R. Jemian, *Irena: tool suite for modeling and analysis of small-angle scattering.* Journal of Applied Crystallography, 2009. **42**(42): p. 347-353.
14. Ilavsky, J., *Nika: software for two-dimensional data reduction.* Journal of Applied Crystallography, 2012. **45**: p. 324-328.
15. Peterson, P.D., J.T. Mang, and B.W. Asay, *Quantitative analysis of damage in an octahydro-1,3,5,7-tetranitro-1,3,5,7-tetrazonic-based composite explosive subjected to a linear thermal gradient.* Journal of Applied Physics, 2005. **97**: p. 093507.
16. Yan, G.Y., et al., *A small-angle X-ray scattering study of micro-defects in thermally treated HMX.* Acta Physica Sinica, 2012. **61**(13).
17. Mang, J.T., et al., *An optical microscopy and small-angle scattering study of porosity in thermally treated PBX 9501*, in *Shock Compression of Condensed Matter-2001, Pts 1 and 2, Proceedings*, M.D. Furnish, N.N. Thadhani, and Y. Horie, Editors. 2002, Amer Inst Physics: Melville. p. 833-836.
18. MacDowell, A.A., et al., *X-ray micro-Tomography at the Advanced Light Source.* Developments in X-Ray Tomography Viii, 2012. **8506**: p. 14.
19. Glatter, O. and O. Kratky, eds. *Small Angle X-ray Scattering*. 1982, Academic Press Inc.: London. 515.
20. Saw, C.K. in *The 12th International Detonation Symposium*. 2002. San Diego, CA.
21. Xue, C., et al., *The beta-delta-Phase Transition and Thermal Expansion of Octahydro-1,3,5,7-Tetranitro-1,3,5,7-Tetrazocine.* Propellants Explosives Pyrotechnics, 2010. **35**(4): p. 333-338.

22. Berghout, H.L., et al., *Combustion of damaged PBX 9501 explosive.* Thermochimica Acta, 2002. **384**(1-2): p. 261-277.
23. Saw, C.K. and C.M. Tarver, *Binder/HMX interaction in PBX9501 at elevated temperatures*, in *Shock Compression of Condensed Matter - 2003, Pts 1 and 2, Proceedings*, M.D. Furnish, Y.M. Gupta, and J.W. Forbes, Editors. 2004, Amer Inst Physics: Melville. p. 1029-1032.
24. Willey, T.M., et al. *The Mesoscale Evolution of Voids in HMX-based Explosives During Heating Through the beta-delta Phase Transition*. in *Proceedings of The 15th International Detonation Symposium*. 2014. San Francisco, California, USA.

"Mesoscale Evolution of Voids and Microstructural Changes in HMX-based Explosives during Heating Through the β-δ Phase Transition"

Supporting Information

Trevor M. Willey, Lisa Lauderbach, Franco Gagliardi, Tony van Buuren,

Elizabeth A. Glascoe, Joseph W. Tringe, Jonathan R. I. Lee, Keo Springer, and

Jan Ilavsky

1. Supplementary Figures

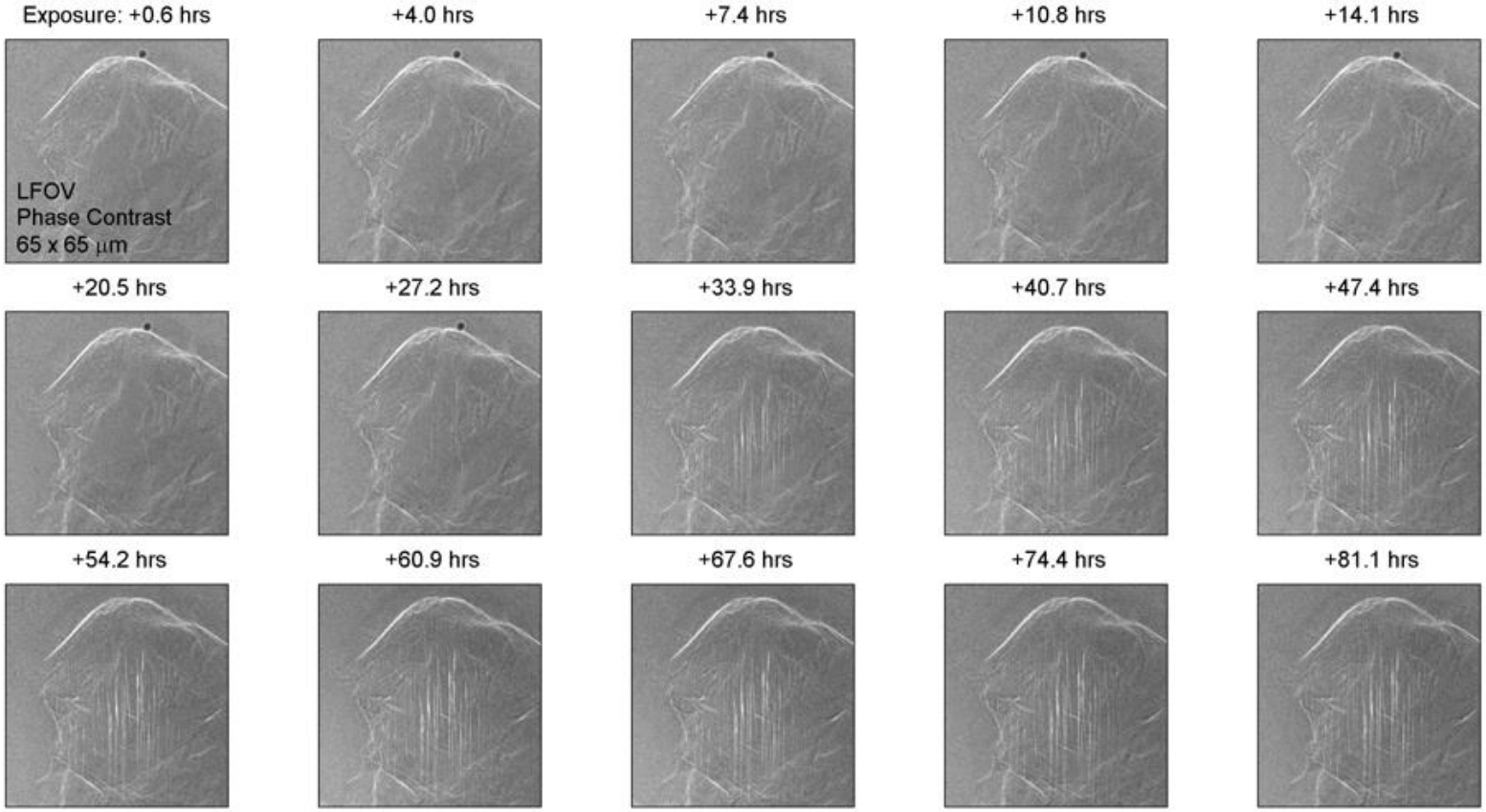

Figure SF1: A series of images acquired from an X-radia Nanotomography instrument while continuously rotating a single HMX crystallite under continuous x-ray illumination. All images are presented from a particular angle and acquired at the indicated times. Apparent in the images are phase-contrast from planar fissures developing in the crystallite under x-rays. Significantly, the width of the fissures are consistent with the length scales of the Guinier observed with x-ray beam damage in the USAXS data. Data acquired and courtesy of Chuck Divin, LLNL

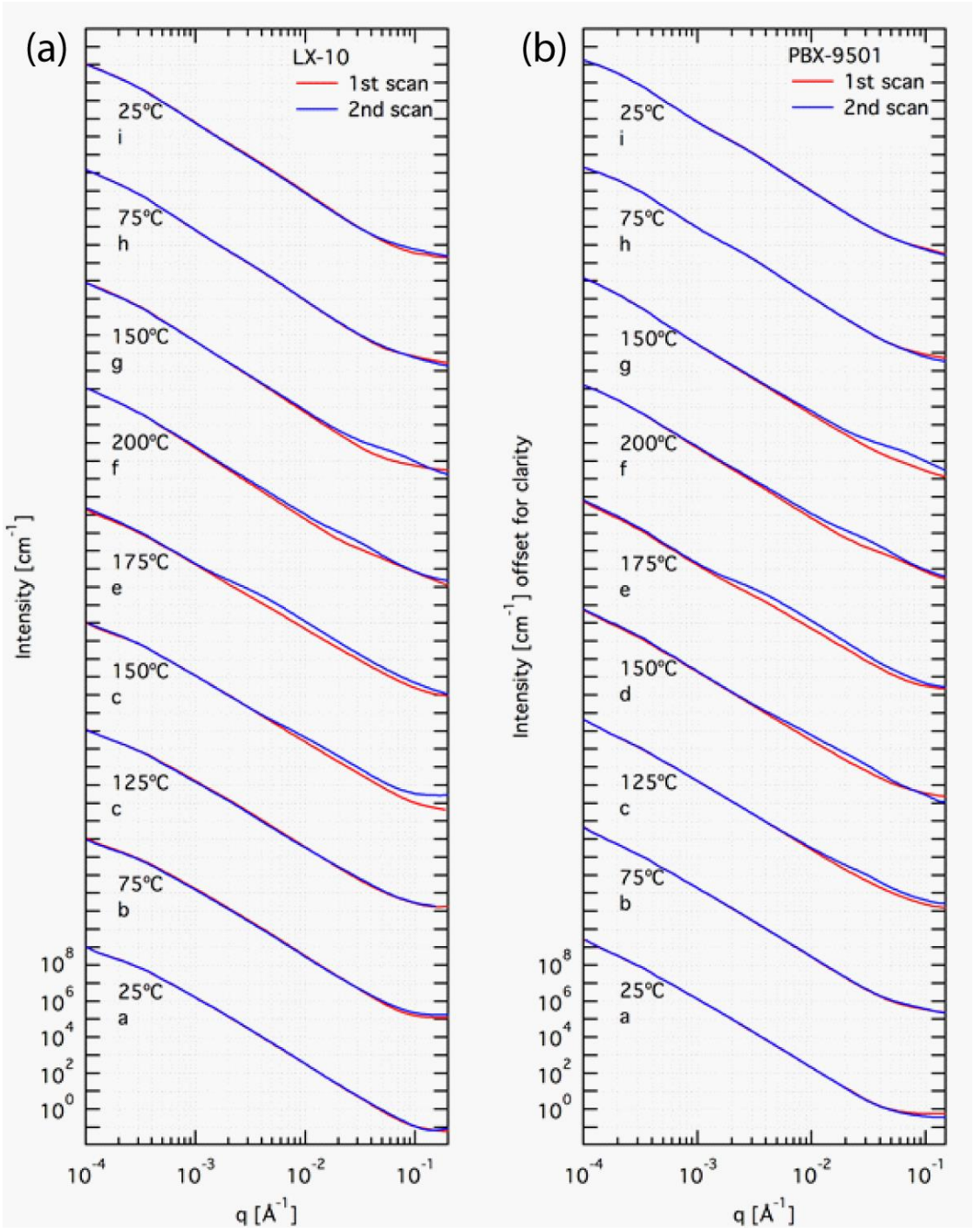

Figure SF2: Ultra-small angle x-ray scattering from **(a)** LX-10 and **(b)** PBX-9501 during the temperature cycles of Fig. 2 in the main text. The red and blue scans were acquired in rapid succession at each temperature. As observed in Fig.1 of the main manuscript, the x-ray damage feature moves from high-q towards lower q and appears to be dependent upon both temperature and dosage. Comparison of (a) and (b) indicates that the δ-phase exhibits less rapid beam damage**.**

2. Supplementary Movies

All of the captions presented in this section correspond to movies available online as supporting information files.

Movie SM1 Caption: Optical microscopy of LX-10 subjected to approximately the same temperature cycle as the USAXS scans presented in the main manuscript and this supporting information document. The sample was placed slightly off-center so that ramping in temperature can be detected in the movie itself by the sample moving within the field-of-view. The movement in the sample is due to thermal expansion of the heating stage. Several key frames of this movie are provided in Fig. 4 of the main text.

Movie SM2 Caption: Rotating view of an XCT generated 3D rendering of an LX-10 sample prior to heating. One image of this movie is included in figure 6 of the main manuscript.

Movie SM3 Caption: Rotating view of an XCT generated 3D rendering of an LX-10 sample after thermal annealing. The thermal annealing was consistent with the treatment applied to samples used in collection of the USAXS data displayed in figure 1 of the main manuscript and figure S2 of this supporting information document. One image of this movie is included in figure 6 of the main manuscript.

Movie SM4 Caption: Rotating view of an XCT generated 3D rendering of a PBX-9501 sample prior to heating. One image of this movie is included in figure 6 of the main manuscript.

Movie SM5 Caption: Rotating view of an XCT generated 3D rendering of a PBX-9501 sample after thermal annealing. The thermal annealing was consistent with the treatment applied to samples used in collection of the USAXS data displayed in figure 1 of the main manuscript and figure S2 of this supporting information document. One image of this movie is included in figure 6 of the main manuscript.